



HAL
open science

Dynamic Characterization of III-Nitride-Based High-Speed Photodiodes

Bandar Alshehri, Karim Dogheche, Sofiane Belahsene, Abderrahim Ramdane, Gilles Patriarche, Didier Decoster, El Hadj Dogheche

► **To cite this version:**

Bandar Alshehri, Karim Dogheche, Sofiane Belahsene, Abderrahim Ramdane, Gilles Patriarche, et al.. Dynamic Characterization of III-Nitride-Based High-Speed Photodiodes. *IEEE Photonics Journal*, 2017, 9 (4), pp.6803006. 10.1109/JPHOT.2017.2714168 . hal-03552276

HAL Id: hal-03552276

<https://uphf.hal.science/hal-03552276v1>

Submitted on 12 Jun 2024

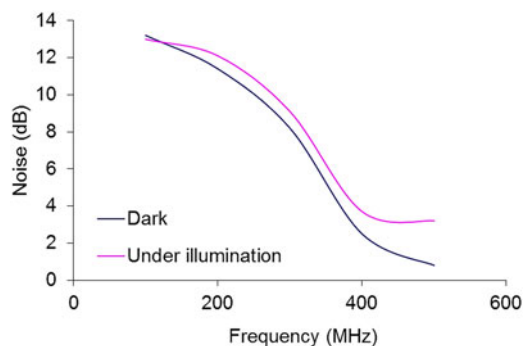
HAL is a multi-disciplinary open access archive for the deposit and dissemination of scientific research documents, whether they are published or not. The documents may come from teaching and research institutions in France or abroad, or from public or private research centers.

L'archive ouverte pluridisciplinaire **HAL**, est destinée au dépôt et à la diffusion de documents scientifiques de niveau recherche, publiés ou non, émanant des établissements d'enseignement et de recherche français ou étrangers, des laboratoires publics ou privés.

Dynamic Characterization of III-Nitride-Based High-Speed Photodiodes

Volume 9, Number 4, August 2017

Bandar Alshehri
Karim Dogheche
Sofiane Belahsene
Abderrahim Ramdane
Gilles Patriarche
Didier Decoster
Elhadj Dogheche



DOI: 10.1109/JPHOT.2017.2714168

1943-0655 © 2017 IEEE

Dynamic Characterization of III-Nitride-Based High-Speed Photodiodes

Bandar Alshehri,¹ Karim Dogheche,¹ Sofiane Belahsene,²
Abderrahim Ramdane,² Gilles Patriarche,² Didier Decoster,¹
and Elhadj Dogheche¹

¹Institute of Electronics, Microelectronics & Nanotechnology, Optoelectronics Group (IEMN
CNRS UMR 8520), Villeneuve d'ascq, 59655, France

²C2N, Centre for Nanoscience and Nanotechnology, CNRS, Route de Nozay,
91460 Marcoussis, France

DOI:10.1109/JPHOT.2017.2714168

1943-0655 © 2017 IEEE. Translations and content mining are permitted for academic research only.
Personal use is also permitted, but republication/redistribution requires IEEE permission.
See http://www.ieee.org/publications_standards/publications/rights/index.html for more information.

Manuscript received May 4, 2017; revised June 6, 2017; accepted June 7, 2017. Date of publication June 9, 2017; date of current version June 29, 2017. This work was supported in part by the U.S. Department of Commerce under Grant BS123456. Corresponding author: B. Alshehri (e-mail: bandar.alshehri@iemn.univ-lille1.fr).

Abstract: The objective of this study is to study, design, and develop a high-speed PIN photodiode based on $\text{In}_x\text{Ga}_{1-x}\text{N}/\text{GaN}$ alloys deposited by metal-organic chemical vapor deposition. The configuration used for the PIN photodiode is based on an absorbing layer composed of $\text{In}_{0.1}\text{Ga}_{0.9}\text{N}$ multiple quantum wells. Structural, microstructural, and optical analyses have been carried out using TEM, PL, and absorption measurement. The design of PIN structures varies with an active surface ranging from 10^4 to $10^6 \mu\text{m}^2$. Static and dynamic characterizations have been performed to qualify the photodiode response. A photocurrent value reaching a maximum of 1.2 mA is reported for a diode of $100 \times 100 \mu\text{m}^2$ area, with an external quantum efficiency of 13%. Using the noise measurement technique, the device reveals a -3 -dB cutoff frequency of 300 MHz for the same photodiode. This result clearly shows the potential of III-nitride materials for targeting high-speed optoelectronics. The future prospect is to work toward InGaN-based microphotodiodes in order to achieve optical transmission links in the UV-visible range using the same material system.

Index Terms: Photodetectors, GaN, bandwidth, fabrication and characterization.

1. Introduction

III-Nitride semi-conductor materials have attracted a lot of interest for new generation of optoelectronic devices [1]. The advantage with these materials is the flexible bandgap varying from 0.7 to 6 eV hence covering an ultra-broad spectrum, from deep ultraviolet up to near infrared [2], allowing the development of numerous applications. Solar cells based on nitride materials have readily been investigated for terrestrial and space-based applications [3]. Transistors performance for high power electronics, ground-based communications and biological agent detection devices has been enhanced [4]. Major efforts have been dedicated to the technological fabrication in order to achieve efficient emitters and detectors [5]. Recent progress has demonstrated cutting-edge results in high-speed data rate connectivity and integrated circuits [6]. Imaging sensors based on high speed electronics have been implemented based on their sensitive applications in security screening [7]. Gallium nitride (GaN) as a member of III-nitride family has become the revolutionary

material owing to its electronic and optical properties. Direct, flexible and wide bandgap of GaN makes this material a key candidate for achieving high frequency, bandwidth, power and efficiency devices. GaN based detectors are in particular suitable for full color display, high density information storage, and UV-VIS communication links [8].

Among the most important optical properties that GaN and related alloys exhibit is the absorption coefficient which directly determines device operation. Its measured value is about 10^5 cm^{-1} , much higher than that of GaAs (10^4 cm^{-1}) and Si (10^3 cm^{-1}) near the band edge [9]. GaN-based alloys are very promising as they can deliver higher critical field compatible with higher power densities as well as higher electron saturation velocities and consequently ultrafast transition times, leading to higher operating frequencies.

In the past, many efforts have been devoted to the achievement of higher output power, efficiency and cut-off frequency [10], [11]. Basically, the main limitations for accomplishing these objectives are the saturation under high injection regime, the intrinsic bandwidth and the coupling between the RF power and the antenna [12], [13].

In the literature, authors report some studies related to time as well as frequency response of PIN UV photodetectors. From single crystal GaN, Carrano *et al.* [14] have measured a rise-time of ~ 43 psec at 15 V reverse bias voltage for a mesa diameter of $60 \mu\text{m}$ and $1 \mu\text{m}$ thick InGaN intrinsic region. Authors indicate that PIN photodetectors are mostly transit-time limited for small area while they are RC-limited for larger area due to parasitic capacitances. The same group has reported fast PIN photodiodes with time responses shorter than 1 ns at -5 V bias voltage [15]. This result demonstrates that lowering the device capacitance requires a thicker intrinsic InGaN layer (thickness up to $1 \mu\text{m}$). Therefore, the transit time of the carriers is the main factor limiting the time response instead of the RC factor. The disadvantage of Carrano's structure consists in its low responsivity value (30 mA/W at -5 V) since the intrinsic region is thicker than the diffusion length of the carriers. In our study, we have applied a bias voltage of -5 V in order to deplete completely the intrinsic layer (thickness of 145 nm). Therefore, as the intrinsic layer is very thin, one can consider here that the behavior of the photodiode is similar to a classical PIN structure. The transport is governed by the transit of the carrier across the intrinsic layer. In this condition, photocurrent is saturated at the bias voltage of -5 Volts.

The photodiode is currently one of the most popular device used for light detection. Its external quantum efficiency (*EQE*) describes the number of electron/hole pairs generated by absorbed photons participating in the photocurrent. EQE is calculated using the formula:

$$EQE = R \times \frac{hc}{q\lambda} \quad (1)$$

Where R is the responsivity at the wavelength λ , h the Planck's constant, c the speed of light and q the electron charge. The cut-off frequency at -3 dB related to RC time constant is expressed as following:

$$F_{RC} = 1/2\pi RC \quad (2)$$

Where R is the global resistance of photodiode and the load resistance and the capacitance $C = \frac{\epsilon S}{e}$ with S is the photodiode surface and e the thickness of the active layer. This work aims to study the relation between the device dimensions and the frequency behavior for GaN materials.

2. Experiments

The proposed PIN structure consists of a thick not-intentionally-doped (n.i.d) GaN buffer layer (called also undoped GaN) on c-plane (0001) sapphire. In order to ensure a high crystalline quality GaN and to move away from the GaN/Sapphire interface, the thickness of this layer is chosen to be $2.5 \mu\text{m}$. This is followed by a $3.5 \mu\text{m}$ thick Si-doped n-type GaN layer with a carrier concentration of $3 \times 10^{18} \text{ cm}^{-3}$.

The thickness of the "i" intrinsic- absorption- layer, is $\sim 145 \text{ nm}$ in order to efficiently absorb the incident light. The MQW structure is grown with ten pairs of InGaN/GaN with thicknesses of 2.5 nm

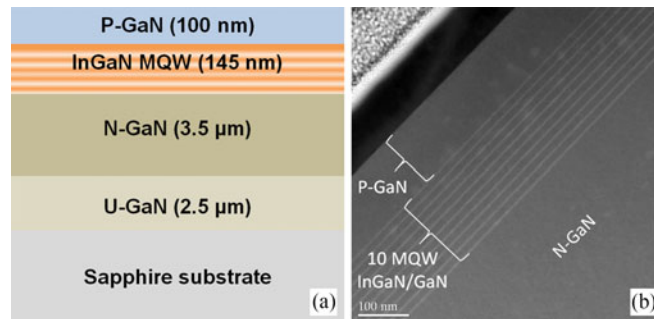


Fig 1. (a) PIN structure, (b) TEM analysis for InGaN/GaN.

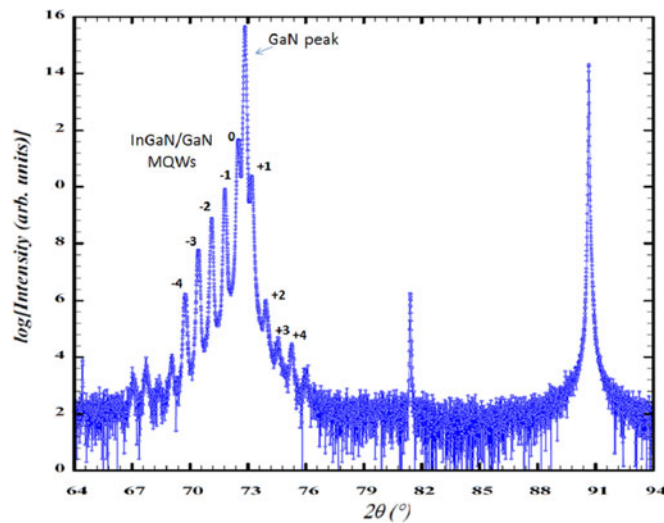


Fig 2. XRD scan measurement for MQW structure grown by MOCVD.

for InGaN and 12 nm for GaN within the InGaN/GaN well. 100 nm Mg-doped p-type GaN layer is grown as the top layer with a carrier concentration of $5 \times 10^{17} \text{ cm}^{-3}$ as shown in Fig. 1.

InGaN/GaN MQW configuration exhibits less strain stress in the structure, resulting in a better material quality compared to an InGaN single layer deposited on top of a GaN template. Note that in a previous study [17], we have studied both configurations from XRD, PL and TEM analysis. The microstructure will reveal an improved quality for InGaN/GaN MQW compared to the single thick layer: this is mainly due to the significant reduction of threading dislocation.

The analysis of structural and the optical properties have been performed in order to investigate the crystalline quality from X-ray Diffraction (XRD) and density of dislocation and surface morphology from TEM. The XRD analysis indicate that the InGaN is highly oriented along the c-axis with sharp and narrow peak. The high intensity peak observed clearly at 72.7° corresponds to the thick GaN buffer layer beneath the PIN structure, which indicates that the GaN is highly oriented along the c-axis (see Fig. 2). For the InGaN/GaN MQW, it exhibits satellite peaks, the position and the intensity of peak is changing due the unexpected interfaces change of wells in the InGaN/GaN period. The series of peaks (satellite peaks) numbered from -4 to $+4$ could provide information about indium composition, period numbers and well thickness. The position of main MQW peak (position "0") enables the calculation of the average indium content in the InGaN/GaN period and not the indium content in the InGaN layer.

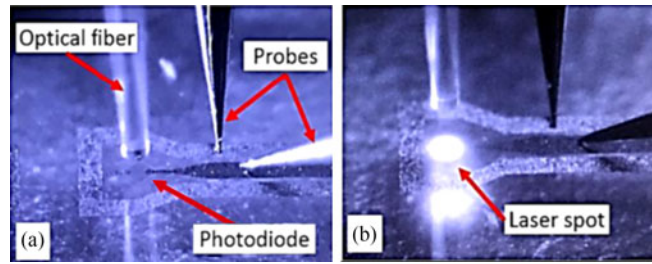


Fig. 3. Image issued from super-zoom HD camera showing coplanar photodiode (a) in dark measurement (b) under illumination.

We will consider that MQW layers are assumed to be relaxed in order to determine the indium composition. The approximation of Indium content is obtained by comparison of measured curve with a simulated structure using LEPTOS software. The type of XRD measurement for this comparison is a rocking curve omega measurement and the average indium percentage is about 12%. The Full width at half maximum (FWHM) for InGaN is about 405 arcseconds due to the period interface roughness and may also be related to the alloy fluctuation.

Fig. 1(b) reveals the improved quality owing to the significant reduction of threading dislocations (10^8 cm^{-2}). Optical properties have been evaluated using Photoluminescence (PL) and absorption measurement in order to obtain the cut-off wavelength. These have shown a sharp single PL peak corresponding to near-band edge transition in the epitaxial MQW InGaN phase at 425 nm (2.91 eV) with a narrow FWHM of 14 nm. This value has been confirmed by the absorption measurement for the InGaN layer absorption coefficient of 1.6×10^5 almost similar to the reported values [16].

Fabrication process of photodiode consists of four steps starting by p-type top contact deposition, etching process to reach n-GaN layer, n-type contact deposition and finally thermal annealing of n and p contacts. Metals have been optimized to be Pd/Au with respective thicknesses of 35 nm/120 nm for p-type top contact demonstrating the high work function of Pd metal associated with its high reactivity with low contact resistance [17]. Ti/Al/Au metals with respective thicknesses of 10 nm/30 nm/300 nm for n-type bottom contact have been used [18].

The measurement of photocurrent relies on two important factors, the wavelength of incident light and the output power. For this reason, a laser source has been used for powerful input light. Besides, fiber-coupled laser source is the optimal choice due to the ease to focus a laser beam using stripped and cleaved optical fiber (see Fig. 3). The wavelength of fiber-coupled laser source is 405 nm and its output power reaches 100 mW.

In order to estimate the cut-off frequency, we have first theoretically calculated it from the average value of the capacitance C . Previously, we have investigated the capacitance values using a C-V setup, for photodiode areas ranging from $100 \times 100 \mu\text{m}^2$ to $1000 \times 1000 \mu\text{m}^2$. The extraction of capacitance permits us to estimate the cut-off frequency and compare these results to the theoretical values. This approach gives some indications in order to optimize the design of the photodiodes and more generally to reduce the capacitive effects. To the best of our knowledge, no method exists that allows the direct measurement of the photodiode cut-off frequency in UV-Vis region. For the frequency experiments, due to the lack of modulated laser source (in the wavelength range 400 to 633 nm), we have performed noise figure techniques already used for III-V semiconductors technologies samples but in the IR range. This experiment is related to the noise figure measurement. Briefly, among the different noise components (thermal noise, shot noise, transit-time noise, etc.), the most important one is the shot noise for the photodiode. This noise is mainly due to the velocity distribution of the carriers. Shot noise should vary according to the photodiode current, while the thermal noise related to the photodiode and the Noise-Figure-Meter should be constant. The experiment is performed using the photocurrent measurement set-up with laser source ($\lambda = 405\text{nm}$) as incident light; the Noise-Figure-Meter is connected to the RF probes and signal generator. RF probes and laser spot are adjusted on the photodiode with Superzoom HD camera, lamp and related screen display. Coplanar transmission lines have

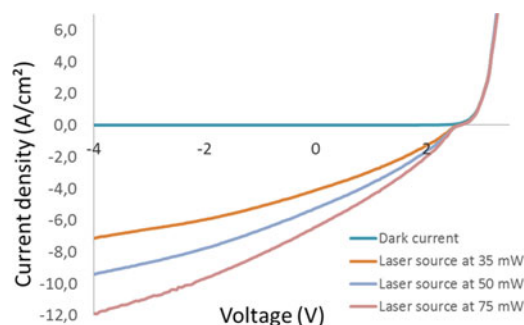


Fig 4. I-V characteristics for dark and photocurrent measurements at different laser powers.

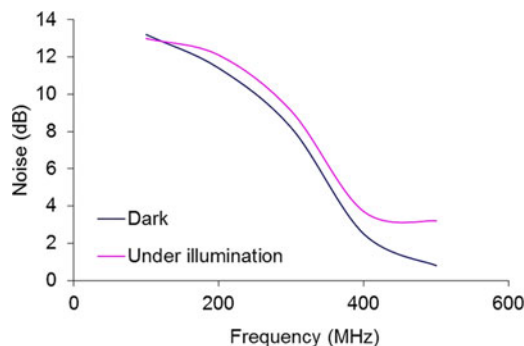


Fig 5. Noise measurement for $100 \times 100 \mu\text{m}^2$ photodiode using Noise-Figure-Meter technique.

been designed and fabricated on top of the samples. Measurements are performed under reverse bias both in the dark and under illumination by laser source. This method is considered as one of the most convenient technique to extract the cut-off frequency for photodiodes. It consists in the noise measurement as function of the frequency. This method has been used by Gouy [19] for InP photodiode at $\lambda = 1.5 \mu\text{m}$. The evolution of noise response clearly indicates a limitation in the photodiode behavior when the frequency increases, allowing the estimate of the 3 dB cut-off frequency, a very convenient way to assess the dynamic response of fabricated photodiodes.

3. Measurement Results and Discussion

Samples with different dimensions have been investigated by photocurrent measurement in order to evaluate the photodiode response. For each measurement, we have evaluated the dark current followed by three photocurrents at the following output laser powers of 35, 50 and 75 mW. Fig. 4 exhibits the dark measurement and it is compared to photocurrent measurements at different laser power (photodiode dimension of $100 \times 100 \mu\text{m}^2$). The photocurrent value increases with laser power and it attains a maximum of 1.2 mA at -4 V equivalent to 12 A/cm^2 ; for nominal laser power of 75 mW. The leakage current of dark measurement is evaluated at around 531 nA at -4 V equivalent to 0.0053 A/cm^2 . The related EQE value achieves a maximum of 13%.

The investigation of size-dependent capacitance has been performed for large-scale photodiodes (from 100×100 to $1000 \times 1000 \mu\text{m}^2$) using a C-V setup. The capacitance is proportional to the photodiode size and particularly to the diameter of the mesa produced by dry etching. The cut-off frequency related to RC time constant is extracted using reported capacitance as a function of mesa dimensions. Results show an estimated cut-off frequency of 390 MHz for a mesa of $100 \times 100 \mu\text{m}^2$. Conversely, the lower cut-off frequency of 9 MHz is observed for $1000 \times 1000 \mu\text{m}^2$ demonstrating the influence of the capacitance on the dynamic response.

Fig. 5 shows the evolution of the noise intensity as function of frequency: we have selected a photodiode with $100 \times 100 \mu\text{m}^2$ and using coplanar lines for the probe connection. The photodiode

TABLE 1
Comparison of Cut-Off Frequency Issued Using Theoretical Calculation, C-V Measurement and Noise Measurement

Photodiode Surface	$FC_{\text{Theoretical}}$	$FC_{\text{via C-V}}$	$FC_{\text{via Noise}}$
$100 \times 100 \mu\text{m}^2$	410 MHz	390 MHz	300 MHz

has been biased under reverse voltage in dark and under illumination of laser source in order to measure the shot noise. The curve shows a drop of shot noise related to the photodiode current when frequency is increased. The difference in noise intensity between dark (N_{dark}) and under illumination ($N_{\text{photocurrent}}$) is detected and observed very small when bias voltage of -4 V is applied for small photodiode dimensions. The difference ($N_{\text{photocurrent}} - N_{\text{dark}}$) in average value is roughly about 0.8 dB. From Fig. 4, the -3 -dB cut-off frequency is estimated to be 300 MHz for a photodiode diameter of $100 \mu\text{m}$.

The reported value of the cut-off frequency using noise measurement is compared to that calculated theoretically from (2) as well as value calculated through C-V measurements. Table 1 shows the reported values of cut-off frequencies for $100 \times 100 \mu\text{m}^2$. The theoretically calculated value is higher than the measured ones because calculation does not take into account metal coplanar lines which add circuit of inductance and related capacitances. This leads to parasitical capacitance and consequently the reduction of frequency limit. The calculated value from the capacitance C-V is close to the value deduced from noise measurement even though the coplanar lines slightly reduce the cut-off frequency.

4. Conclusion

In this study, design, material characterization and device fabrication have been performed for InGaN/GaN based photodiodes. The InGaN absorbent layer has been defined with 10% of indium content. The objective of this work has been directed towards fabrication of high speed photodiodes. The first step of this work is to optimize the photodiode design and fabrication in order to reduce the capacitive effects. Firstly, large-scale photodiodes have been employed to extract the photocurrent and the cut-off frequency. The increase of photocurrents is observed once the laser power is increased and attains 1.2 mA equivalent to 12 A/cm^2 ; with EQE value of 13%. Theoretical calculation of the photodiode frequency has been performed in order to compare it with the experimented values issued from C-V setup and Noise measurement. Results demonstrate a cut-off frequency at -3 dB of 300 MHz using Noise measurement for $100 \times 100 \mu\text{m}^2$ photodiode. This result paves the way to higher frequency for device dimensions up to $20 \mu\text{m}$. This study offers the possibility to work toward InGaN-based μ -Photodiodes such as a perspective work. It could be the photodetector/receiver for the recent InGaN-based μ -LED [20].

Acknowledgment

The authors would like to thank Dr. H. Alyoussefi, and N. Alsubaie, from Taqnia Riyadh for their continuous encouragements.

References

- [1] S. Nakamura, T. Mukai, and M. Senoh, "Candela-class high-brightness InGaN/AlGaIn double-heterostructure blue-light-emitting diodes," *Appl. Phys. Lett.*, vol. 64, no. 13, p. 1687, 1994.

- [2] A. Castiglia, M. Rossetti, M. Duell, C. Vélez, and N. Grandjean, "InGaN laser diodes emitting at 500 nm with p-layers grown by molecular beam epitaxy," *Appl. Phys. Exp.*, vol. 8, p. 22105, 2015.
- [3] J. Wu *et al.*, "Superior radiation resistance of In_{1-x}Ga_xN alloys: Full-solar-spectrum photovoltaic material system," *J. Appl. Phys.*, vol. 94, no. 10, pp. 6477–6482, 2003.
- [4] U. K. Mishra, L. Shen, T. E. Kazior, and Y. F. Wu, "GaN-based RF power devices and amplifiers," *Proc. IEEE*, vol. 96, no. 2, pp. 287–305, Mar. 2008.
- [5] D. Walker *et al.*, "Al_xGa_{1-x}N (0 ≤ x ≤ 1) ultraviolet photodetectors grown on sapphire by metal-organic chemical-vapor deposition," *Appl. Phys. Lett.*, vol. 70, no. 8, p. 949, 1997.
- [6] S. Zhang *et al.*, "1.5 Gbit/s multi-channel visible light communications using CMOS-Controlled GaN-Based LEDs," vol. 31, no. 8, pp. 1211–1216, 2013.
- [7] C. Skierbiszewski, "Growth and characterization of AlInN/GaN quantum wells for high-speed intersubband devices at telecommunication wavelengths," *Proc. SPIE*, vol. 6121, no. 2006, pp. 612109-1–612109-12, 2006.
- [8] E. Muñoz *et al.*, "III nitrides and UV detection," *J. Phys. Condens. Matter*, vol. 13, pp. 7115–7137, 2001.
- [9] H. Morkoç, *Nitride Semiconductors and Devices*. Berlin, Germany: Springer-Verlag, 1999.
- [10] S. M. Duffy *et al.*, "Accurate modeling of dual dipole and slot elements used with photomixers for coherent terahertz output power," *IEEE Trans. Microw. Theory Tech.*, vol. 49, no. 6, pp. 1032–1038, Jun. 2001.
- [11] H. Ito *et al.*, "Photonic millimetre-wave emission at 300 GHz using an antenna-integrated uni-travelling-carrier photodiode," *Electron. Lett.*, vol. 38, no. 17, p. 989, 2002.
- [12] B. Alshehri *et al.*, "Synthesis of In_{0.1}Ga_{0.9}N/GaN structures grown by MOCVD and MBE for high speed optoelectronics," *MRS Adv.*, pp. 1–8, 2016.
- [13] M. El Besseghi *et al.*, "Frequency response modeling and optimization of a PIN photodiode based on GaN/InGaN adapted to photodetection at a wavelength of 633 nm," *Mater. Chem. Phys.*, vol. 162, pp. 525–530, 2015.
- [14] J. C. Carrano *et al.*, "Very high-speed metal-semiconductor-metal ultraviolet photodetectors fabricated on GaN," *Appl. Phys. Lett.*, vol. 73, no. 17, pp. 2405–2407, 1998.
- [15] J. Carrano, T. Li, C. Eiting, R. Dupuis, and J. Campbell, "Very high-speed ultraviolet photodetectors fabricated on GaN," *J. Electron. Mater.*, vol. 28, no. 3, pp. 325–333, 1999.
- [16] F. K. Yam and Z. Hassan, "InGaN: An overview of the growth kinetics, physical properties and emission mechanisms," *Superlattices Microstruct.*, vol. 43, no. 1, pp. 1–23, 2008.
- [17] S. Belahsene *et al.*, "Microstructural and electrical investigation of Pd/Au ohmic contact on p-GaN," *J. Vac. Sci. Technol. B, Nanotechnol. Microelectron. Mater. Process. Meas. Phenom.*, vol. 33, no. 1, p. 10603, Jan. 2015.
- [18] J.-P. Shim, M. Choe, S.-R. Jeon, D. Seo, T. Lee, and D.-S. Lee, "InGaN-Based p-i-n solar cells with graphene electrodes," *Appl. Phys. Exp.*, vol. 4, no. 5, p. 52302, May 2011.
- [19] J.-P. Gouy, "Etude comparative de la photodiode PIN de la photodiode a avalanche et du photoconducteur sur materiaux III-V," Ph.D. dissertation, 1989.
- [20] W. Yang *et al.*, "Size-dependent capacitance study on InGaN-based micro-light-emitting diodes," *J. Appl. Phys.*, vol. 116, no. 4, p. 44512, Jul. 2014.